Science of Remote Sensing 1 (2020) 100003

Contents lists available at ScienceDirect

Science of Remote Sensing

journal homepage: www.journals.elsevier.com/science-of-remote-sensing

Full Length Article

A novel method to extract urban human settlements by integrating remote sensing and mobile phone locations

Bin Chen [a,*,1], Yimeng Song [b,1], Bo Huang [c], Bing Xu [d,*]

[a] Department of Land, Air and Water Resources, University of California Davis, CA, 95616, USA
[b] Department of Urban Planning and Design, The University of Hong Kong, Hong Kong
[c] Department of Geography and Resource Management, The Chinese University of Hong Kong, Hong Kong
[d] Ministry of Education Key Laboratory for Earth System Modeling, Department of Earth System Science, Tsinghua University, Beijing, 100084, China

ARTICLE INFO

Keywords:
Urban human settlements
Location-based data
Landsat
MODIS
POIs

ABSTRACT

Satellite-based human settlement extraction methods have limited practical applications, due to merely studying the difference between human settlements and other land cover/use types in physical attributes (e.g., spectral signature and land surface temperature) instead of considering basic anthropogenic attributes (e.g., human distribution and human activities). To deal with this challenge, we proposed a novel method to accurately extract human settlements by integrating mobile phone locating-request (MPL) data and remotely sensed data. In this study, human settlements for selected cities were mapped at a medium resolution (30 m) by redistributing the MPL data using Landsat Normalized Difference Vegetation Index (NDVI) adjusted weights, with an overall accuracy of above 90.0%. Additionally, by extending the proposed method to the MPL and Moderate Resolution Imaging Spectroradiometer (MODIS) data, a coarse-resolution (250 m) map of human settlements in China was created with an overall accuracy of 95.2%. Compared with the widely used nighttime light based methods, the proposed method could solve the long-existing problems such as data saturation and blooming effects, as well as characterizing human settlements with fine spatial details. Our study provides an alternative approach to human settlement extraction by combining its physical and anthropogenic attributes, and it can be easily adjusted with multi-scale remotely sensed data and applied to human settlement extraction at different scales.

1. Introduction

Human settlements typically include cities, towns, villages, and other agglomeration of buildings where people live and work (Ridd and Hipple, 2006). Despite of their small proportion (<1%) covering the land surface (Schneider et al., 2010), human settlements exert a disproportionate influence on their surroundings in terms of mass, energy, and resource fluxes (Cao et al., 2009). Thus, understanding the spatial extent and geographic distribution of human settlements is fundamentally important for landscape management (Zhang et al., 2016), urban planning (Matsuoka and Kaplan, 2008; Pauleit et al., 2005), as well as (i) evaluating the impacts of urbanization on environmental problems such as vegetation loss and degradation (Waseem and Khayyam, 2019), urban heat island effects (Zhou and Chen, 2018), water and air pollution (Shao et al., 2006), and climate change (Carter et al., 2015; Zhou et al., 2004); and (ii) health problems (Xu et al., 2016), such as ambient pollution exposure (Song et al., 2019) and epidemic disease spreading (Tian et al., 2016). All these issues require timely and accurate information on urban human settlements.

Fortunately, satellite remote sensing has greatly facilitated the monitoring and extraction of human settlements by providing spatially explicit and temporally continuous information on dynamic land surface change (Chen et al., 2017). Over the past two decades, numbers of pioneering studies have attempted to extract human settlements using remotely sensed images. Here we classified them into four major categories in terms of the data and methods used in their implementation: (i) optical images; (ii) microwave-based images; (iii) nighttime light images; and (iv) multi-source data integration.

Optical images with high, medium, and coarse spatial resolutions, such as IKONOS, QuickBird, SPOT (Système Probatoire d'Observation de la Terre), Landsat series, and MODIS (Moderate Resolution Imaging Spectroradiometer), have been widely employed for mapping the

* Corresponding authors.
E-mail addresses: bch@ucdavis.edu (B. Chen), bingxu@tsinghua.edu.cn (B. Xu).
[1] These authors contributed equally to this work.

https://doi.org/10.1016/j.srs.2020.100003
Received 18 October 2019; Received in revised form 5 March 2020; Accepted 11 March 2020
Available online 2 April 2020

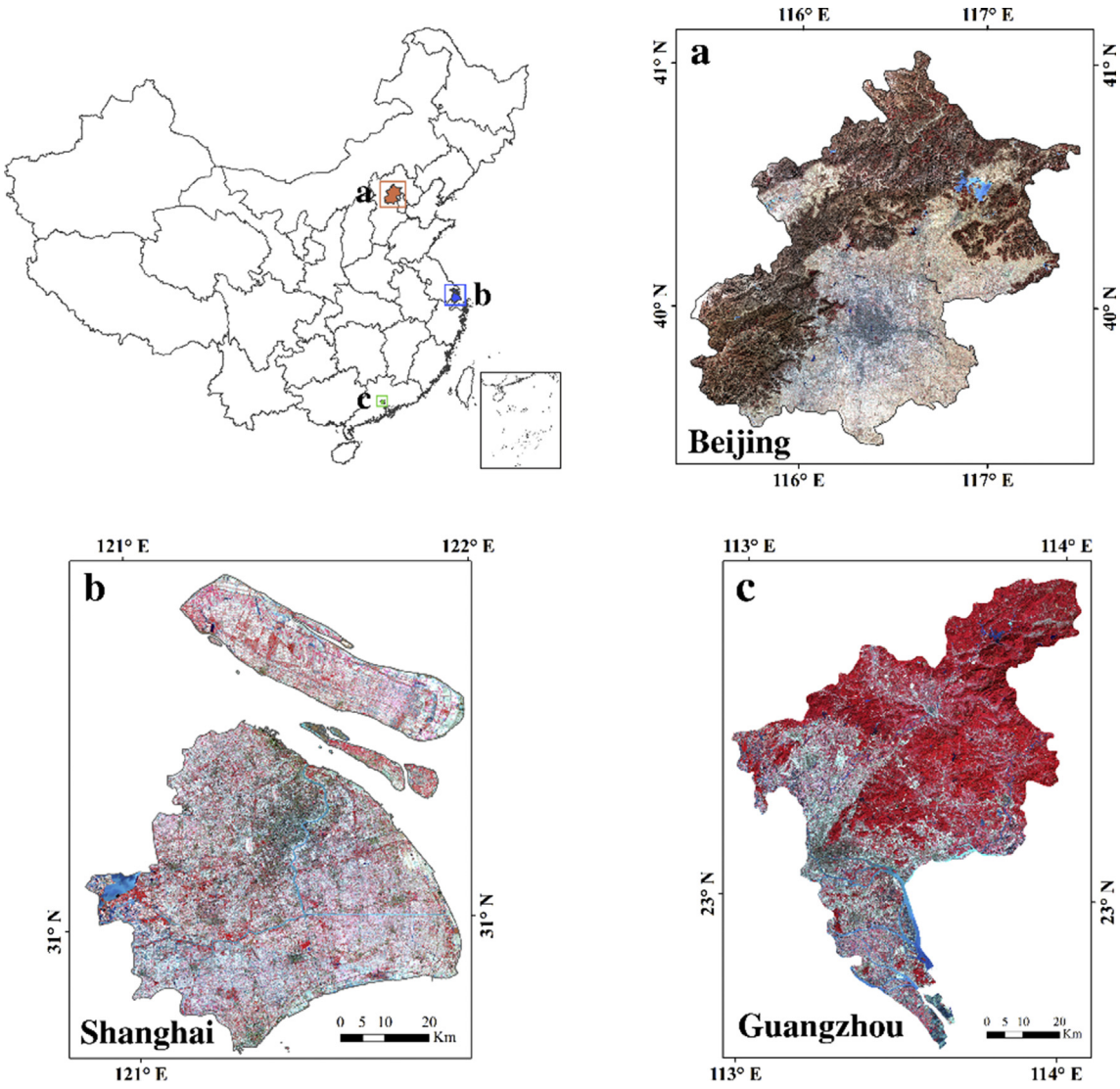

Fig. 1. The geographic locations of three selected cities in China. (a) Beijing, (b) Shanghai, and (c) Guangzhou. The base maps are NIR-red-green composition of Landsat-8 data. (For interpretation of the references to colour in this figure legend, the reader is referred to the Web version of this article.)

magnitude, location, and distribution of human settlement areas from individual-city scale to regional and global scales (Lu et al., 2008; Lu and Weng, 2006, 2009; Patel et al., 2015; Pesaresi et al., 2013; Ridd and Hipple, 2006; Weng, 2012). However, mapping human settlements based on optical images remains challenging due to the following obstacles: firstly, human settlements are commonly composited with artificial facilities built using diverse materials, thereby increasing the intra-class variability and heterogeneity of settlements. They are quite difficult to spectrally separate from other land use types (Li and Gong, 2016; Weng, 2012). Secondly, the sensitivity of optical remote sensing sensors to weather conditions during data acquisition is another primary limitation for information extraction and analysis.

Although less often applied than optical data, microwave-based images have already been popularly discussed for characterizing urban human settlements (Gamba et al., 2011; Pelizari et al., 2018), as a result of (i) the increasing number of High Resolution (HR) and Very High Resolution (VHR) synthetic aperture radar (SAR) sensors, including Envisat ASAR, ALOS PALSAR, RADASAT-1, TerraSAR-X, and Cosmo/Skymed; (ii) the priority of penetrating cloud cover and thus eliminating weather condition impacts on microwave-based data; and (iii) the characteristics of capturing texture and height information. The basic idea for human settlement extraction from SAR data is to differentiate spatial properties through a mix of basic spatial elements to allow labeling scene segments as settlements instead of non-settlements (Gamba et al., 2011). For example, a total of 180,000 TerraSAR-X and TanDEM-X scenes were processed to create the Global Urban Footprint (GUF) product (Esch et al. 2010, 2013) with three land cover types (urban area, land surface, and water). However, the majority of VHR SAR is inaccessible due to the mandated "opportunistic" acquisition policy, thus hindering fine-resolution human settlement extraction at large scales.

Nighttime light images, including DMSP-OLS (the Defense Meteorological Satellite Program's Operational Line-scan System) and Suomi NPP VIIRS (the Suomi National Polar-orbiting Partnership Visible Infrared Imaging Radiometer Suite), have been extensively demonstrated to be a cost-effective data source to indirectly reflect human activities (Cao et al., 2009; Elvidge et al., 2001; Huang et al., 2015; Xie and Weng, 2016; Zhang et al., 2013) and characterize the spatial distribution and dynamic expansion of human settlements (Elvidge et al., 2001; Liu et al., 2012; Weng, 2012; Xie and Weng, 2016). However, nighttime lights are often affected by two sources of noises: saturation effects (nighttime light signals gradually reach saturation in bright urban cores) and blooming effects (the propensity for light to spread into areas surrounding the actual source). Both effects often result in omission in the areas with small proportional settlements such as towns and villages and

overestimation on urban extents, which cause information loss and distortion of spatial patterns (Lu et al., 2008; Zhang et al., 2013).

Mapping human settlements with multi-source data integration has become more and more popular over the past few years. Spectral signatures from optical images such as Landsat, MODIS, and SPOT-VGT were commonly integrated with nighttime light images (DMSP-OLS and VIIRS) to map pixel-based human settlements (Goldblatt et al., 2018; Lu et al., 2008; Zhang et al., 2013). Land surface temperature (LST) data were also combined with optical and nighttime light images to better differentiate human settlement areas with other land cover types (Zhang and Li, 2018; Zhang et al., 2015). Human settlements are sometimes confused with dark objects such as water or shadows in spectral signatures, but their land surface temperatures are different, thus LST-based expert rules can be established to distinguish them. In addition, given the rich spectral signatures from optical images and the detailed texture features from radar data, these two types of data sources were also integrated to better extract human settlement areas (Lu et al., 2011; Salentinig and Gamba, 2015).

However, existing satellite-based human settlement extraction methods have another shortcoming in practical applications, because they merely study the difference between human settlements with other land cover/use types in physical attributes (e.g., spectral signature, texture, and land surface temperature) rather than considering the direct anthropogenic attributes (e.g., human distribution and human activities). Therefore, they cannot successfully differentiate impervious areas without dense agglomeration of human activities (e.g., living or working) apart from the actual human settlement areas. In recent years, the rapid growth of location-based services and social media platforms provides new opportunities to discover the spatial characteristics of human distribution and activities (Cai et al., 2017; Chen et al., 2018b; Song et al., 2018; Steiger et al., 2015). Previous studies have revealed the high correlation between geo-spatial big data (e.g. mobile phone records, social media, taxi trajectories and smart card records) and human distribution (Chen et al., 2018c; Frias-Martinez et al., 2012; Jurdak et al., 2015; Steiger et al., 2015). For example, Chen et al. (2018c) used Tencent-based social media big data to map the global distribution of Chinese population, and Deville et al. (2014) used mobile phone network operators to provide accurate and detailed maps of population distribution at a national scale cost-effectively.

To address the aforementioned limitations of existing methods, we proposed a novel method to extract human settlement areas using real-time mobile phone locating-request (MPL) data from active smart phone users and remote sensing data. Compared with previous methods, the proposed method has the following highlights: (i) characterizing the intrinsic property of human settlements; (ii) integrating mobile phone locations and remote sensing data to produce finer-resolution human settlement maps; and (iii) producing the 250-m human settlement layer derived from mobile phone location-based and remote sensing data in China.

2. Study area and data description

2.1. Study area

As shown in Fig. 1, the study area focuses on three rapidly urbanized cities (Beijing, Shanghai, and Guangzhou) in China. Driven by the effects of politics, economy, science, technology and culture, these three cities with the top GDPs (gross domestic products) have continuous population growth, which leads to the extensive expansion of human settlements over the past decades (Huang et al., 2015). Given the large difference in geographic locations and urban morphology patterns, the selected cities enable us to better verify the effectiveness and robustness of the proposed method.

Beijing, the capital of China, is the biggest city (16,411 km^2) in northern China with a population of more than 21.7 million, and its GDP has reached 414.71 billion US dollars in 2017. Located in the northern China Plain, the flat topography contributed to its rapid urban expansion. As the economic center of China, Shanghai is densely populated with over 24,18 million citizens within an urban area of 6,341 km^2 located in the Yangtze River Delta. In 2017, its GDP was up to 386.45 billion US dollars, roughly 4% of the total GDP in China. As the capital of Guangdong Province, Guangzhou is the largest municipality (7,434 km^2) in southern China with a population of 14.5 million, and its GDP reached 342 billion US dollars in 2017. Similar to Shanghai's superior water-rich location, Guangzhou is situated at the heart of the Pearl River Delta plain, which also experiences a stable ecological environment.

2.2. Mobile phone locating-request big data

In this study, we used the mobile phone locating-request (MPL) data to monitor human movement by retrieving real-time locating requests from mobile phone users' activities in applications (Apps). The MPL data is from Tencent big data platform, which is one of the largest Internet service providers worldwide. All of the MPL data are produced by Tencent company through retrieving real-time locations of active mobile phone users when they are using Tencent Apps and Tencent's location-based services (LBS) called by other mobile Apps. Due to the widespread use of Tencent's service and Apps (e.g., Wechat, QQ, Tencent Map, etc.), the monthly active users of Tencent have reached 700 million, and the daily locating records have reached 36 billion from more than 450 million users globally in 2016 (Tencent, 2016). Thus, the MPL big data could represent unique indicators to characterize human activities at a fine spatiotemporal scale. The dataset used in this study was collected from March 14, 2016, to June 29, 2016, with a spatial resolution of 36 arc-second (~1.2 km) and a temporal resolution of 5-min updating frequency using the application program interface (API) from the Tencent website (http://heat.qq.com). Information regarding users' identities and privacies was removed from the publicly released dataset.

2.3. Landsat series

Landsat level-2 surface reflectance product archived in Google Earth Engine was directly used as the major moderate-resolution data source to redistribute the MPL data. We used the full stack of Landsat-8 Operational Land Imager (OLI) in 2016 that was able to spatially cover each city. Specifically, a total of 149 images from 8 adjacent paths/rows were used for Beijing, a total of 59 images from 2 adjacent paths/rows were used for Shanghai, and a total of 43 images from 2 adjacent paths/rows were used for Guangzhou. We first did a pixel-based quality check to screen and filter out the poor-quality surface reflectance values using cloud mask and quality assessment information in the Landsat metadata, and then we did cloud-free composite over the certain temporal period to generate the base Landsat imagery.

2.4. MODIS data

Two types of MODIS products (MOD09A1 and MOD13Q1) were used in this study. Surface reflectance of MODIS bands 1–7 from MOD09A1 version 6 product was used to calculate remote sensing indexes and verify their potential relationship with location-based data in this study. We redistribute the mobile-phone locating request data using weights derived from Normalized Difference Vegetation Index (NDVI) data to generate human settlement mapping in China. The 16-day composites of NDVI covering the entirety of China were extracted from the MOD13Q1 version 6 product. Both products temporally spanning the entire year were downloaded from the NASA Earth Data portal (https://earthdata.nasa.gov/).

2.5. Social media POIs dataset

Point-of-interests (POIs) represent places or locations with certain functions. People usually go to different POIs for different kinds of purposes,

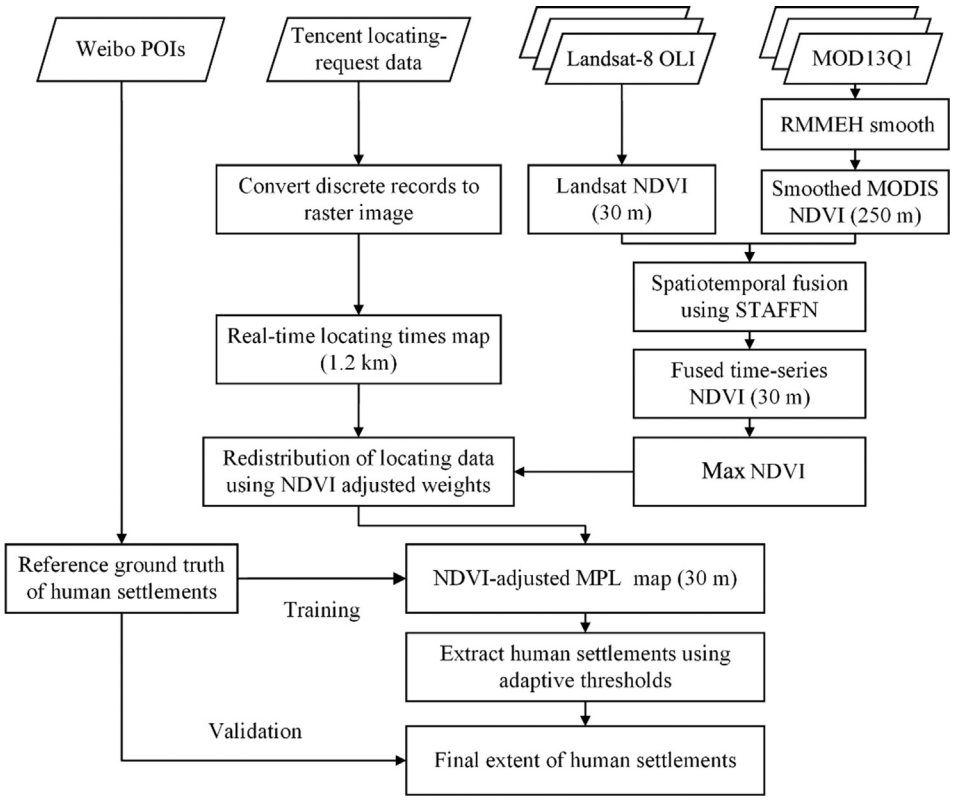

Fig. 2. Flowchart of the research methodology.

e.g., dining, shopping, working, entertaining, etc. POIs extracted from social media check-in records are widely used for identifying human activities and characterizing urban structures (Cai et al., 2017; Kaplan and Haenlein, 2010). The POIs data used in this study were from one of the most popular Chinese social media platforms, Weibo (similar to Twitter). Different from the POIs in other map services (e.g., Google Maps, Baidu Maps, and Tencent Maps, etc.), the related information of Weibo POIs are all recorded by active Weibo's users rather than any other third-party information companies or agencies. When people stay or arrive at a specific place, some of them will make check-in activities using the Weibo App on their smartphones by recording their physical location, the name of the place, and sharing their mood. The dataset with more than 5.4 million POIs was collected through the Weibo API (http://open.weibo.com/) in December 2014. Specifically, each POI record consists of a series of information including location name, coordinates, function category (POIs type), and the number of check−in records. All POIs are classified into nine groups (i.e. Catering, Retailing, Automobile, Accommodation, Recreation, Public Facility, Transportation, Culture & Media, Others). Therefore, in this study, the POIs highly relevant to human daily life were labeled as human settlements based on the category of POIs (Supplementary Table S1) and were used for validation. Although the collected POI dataset had a 2-year difference from other datasets used in 2016, it did not impact much on our validation due to the fact that (i) the POI record was relatively stable and would not change considerably over time; and (ii) the POI dataset was only used to represent human settlements in this study. Even the sub-category of some POI records changed, it still represented human settlements.

3. Methods

Fig. 2 presents a flowchart outlining the methodology applied in this study, including five major procedures as follows. First, data preprocessing was conducted by converting discrete location-based data into raster images, time-series filtering of MODIS data, and converting both Landsat and MODIS into the comparable NDVI data. Second, a self-developed spatiotemporal adaptive fusion model for NDVI products (STAFFN) was used to produce dense time-series NDVI data with moderate spatial resolutions (Chen et al., 2018a). Third, the vegetation index was adjusted to redistribute the coarse-resolution MPL data. Fourth, human settlements were extracted using the adaptive threshold. Fifth, the accuracy validation of extracted human settlements was conducted.

3.1. Data preprocessing

The original MPL dataset was recorded by summing real-time locations of active mobile users using pairs of geodetic coordinates (longitude, latitude). To use this location information, we first constructed a grid with a spatial resolution of 36 arc-second (~1.2 km) (which was consistent with the spatial resolution of MPL data). Using the grid structure, we assigned people to particular grid cells based on the location of their mobile-phone records (Chen et al., 2018c). In this way, the geographic distribution of discrete location records could be presented and visualized using the grid structure of raster images. The MPL data was recorded with a 5-min updating frequency, providing dense time-series dynamics of population movements from hourly to daily, weekly, and monthly temporal scales. We incorporated all the collected MPL records to simulate the general geographic distribution of human beings. Specifically, we first aggregated the 5-min MPL records per day together to produce the daily sum of MPL records, which stood for the daily geographic pattern of human beings, and then averaged all the daily records from March 14, 2016, to June 29, 2016 to get the final MPL layer obtaining the general pattern (Chen et al., 2018c).

As Landsat level-2 surface reflectance product had been calibrated and atmospherically corrected by the Landsat ecosystem distribution adaptive processing system (LEDAPS) (Masek et al., 2013), no further atmospheric correction was required. Thus, the Landsat NDVI imagery was derived from the mosaic surface reflectance data according to Equation (1) (Rouse et al., 1974),

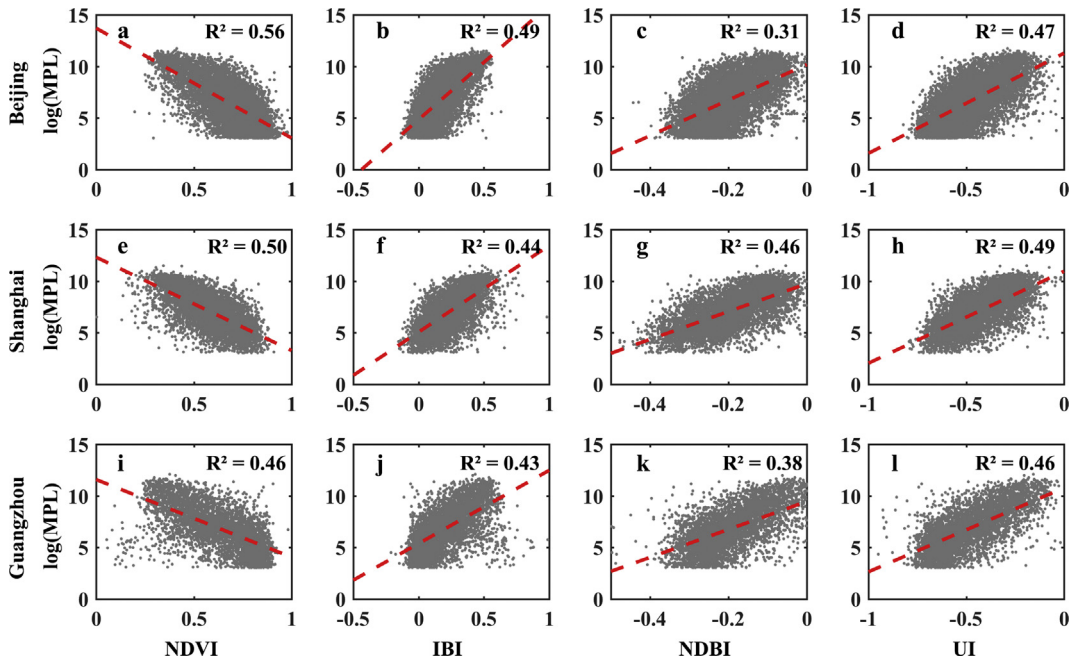

Fig. 3. Correlation between remote sensing metrics (NDVI, IBI, NDBI, and UI) and mobile-phone locating-request times (MPL) in Beijing (a–d), Shanghai (e–h), and Guangzhou (i–l).

$$\mathrm{NDVI} = \frac{NIR - Red}{NIR + Red} \quad (1)$$

where NIR and Red denote the near-infrared band and red band, respectively.

Given the fact that the MOD13Q1 remained significant residual effect from subpixel clouds, variable illumination conditions and viewing geometries, and other remnant errors (Jin and Xu, 2013), in this study, an automated compound smoother, named the Running Median, Mean Value, Maximum Operation, End Point Processing, and Hanning Smoothing (RMMEH) (Jin and Xu, 2013), was adopted to efficiently reduce noise of the MOD13Q1 NDVI time series, and to reconstruct a high quality NDVI time-series dataset. Finally, the MODIS NDVI data were applied and blended with Landsat NDVI imagery to produce a dense time-series and fine-spatial-resolution NDVI dataset.

3.2. Choice of remote sensing index integrated with MPL data

Previous studies have shown that vegetation abundance is closely and inversely correlated with impervious surfaces, which is regarded as an evident characteristic of many urban environments (Small, 2001; Weng et al. 2004, 2006). Generally, in most urbanized regions, the urbanization process results in significant land cover changes from natural vegetation, cultivated land, and bare land to built-up areas. Human activity pattern surveys show that human beings spend an average of 87% of their time in enclosed buildings (Klepeis et al., 2001), and the estimated proportion has reached 90% in developed countries (Klepeis et al., 2001). It is rational to infer that human activities commonly take place in built-up areas or areas of lower vegetation, and we do not expect extensive human activities in densely vegetated areas. In this study, the intensity of human activities is estimated by MPL records. The larger MPL records evidently indicate a higher intensity of human activities. To explore the possible relationship between human activities and remote sensing metrics, we tested the correlation between MPL and the widely used indexes including NDVI, Index-based Built-up Index (IBI) (Xu, 2008), Normalized Difference Built-up Index (NDBI) (Zha et al., 2003), and Urban Index (UI) (Kawamura, 1996). For each city, the remote sensing metrics were calculated from the MOD09A1 greenest composite and then aggregated to the 36-acr-second grids, making their spatial resolution consistent with that of the MPL dataset.

As the pixel-to-pixel scatter plots shown in Fig. 3, it is evident that NDVI and MPL are negatively correlated while the three urban indexes are positively correlated with MPL. Statistical results showed that compared with the other three indexes, NDVI achieved a higher and more robust correlation with MPL for all three cities, i.e., Beijing ($R^2 = 0.56$, $p < 0.001$), Shanghai ($R^2 = 0.50$, $p < 0.001$), and Guangzhou ($R^2 = 0.46$, $p < 0.001$). This experimental test would support the rationale of our assumption that vegetation and human activities are negatively correlated.

3.3. Fusion of landsat NDVI with MODIS NDVI data

Compared with existing spatiotemporal fusion models, the spatio-temporal adaptive fusion model for NDVI products (STAFFN) is proposed to improve blending highly resolved spatial and temporal information from multiple sensors (Chen et al., 2018a). This model integrates an initial prediction into a hierarchical selection strategy of similar pixels, and can capture temporal changes very well. Landsat NDVI data (30 m) was assigned as the base-date Landsat scene, and the resampled MODIS NDVI data (30 m) was temporally closest to Landsat data assigned as the base-date MODIS scene. Then, we applied STAFFN to produce 16-day Landsat-like NDVI time series spanning the entire year from August 2015 to July 2016, by fusing fine temporal information from MODIS and fine spatial information from Landsat data. For redundancy reduction and computational efficiency, the pixel-based maximum NDVIs were extracted from the one-year fused NDVI time series in this study.

3.4. Redistributing coarse-resolution MPL data using NDVI adjusted weights

Inspired by previous studies using vegetation index to downscale nighttime light data for improved urban variability (Zhang et al., 2013), we proposed to redistribute the coarse-resolution location data using the NDVI adjusted weights. In this study, we defined NDVI adjusted locating-request times (NAL) data through Equations (2) and (3). The schematic diagram of implementing NAL is illustrated in Fig. 4. As described above, pixels with larger NDVI values should contribute less to

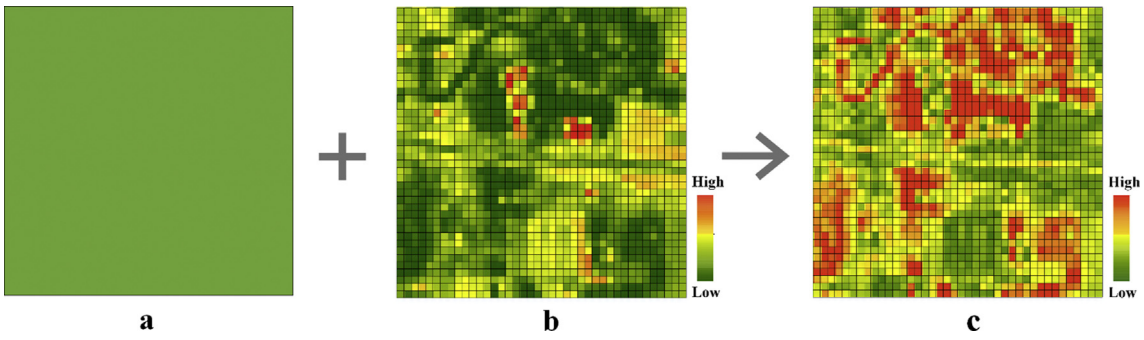

Fig. 4. Schematic diagram of redistributing the coarse-resolution MPL data using NDVI adjusted weights. (a) original MPL data (~1.2 km) at a pixel scale, (b) the fused Landsat NDVI data (30 m) in the same geographic region, and (c) the redistributed fine-resolution MPL data (30 m) derived from (a) and (b).

proportionate the coarse-resolution locating-request times, therefore we used the normalized reciprocal of NDVI as the adjusted weight W_i (range from 0 to 1):

$$W_i = \frac{1/\mathrm{NDVI}_i}{\sum_{i}^{w \cdot w} 1/\mathrm{NDVI}_i}, \quad 0 < \mathrm{NDVI}_i \leq 1 \tag{2}$$

$$\mathrm{NAL}_i = \mathrm{L} \cdot W_i \tag{3}$$

where L denotes the total number of locating-request times for each coarse-resolution MPL pixel (Fig. 4a), NDVI_i is the ith pixel of the fine-resolution maximum NDVI data (Fig. 4b) derived from the Landsat data in Section 3.1. w is the spatial-resolution difference between the locating-request times and NDVI data, and w is 40 in this study. NAL_i denotes the corresponding ith pixel of the redistributed locating-request times data (Fig. 4c). As the negative or zero NDVIs are usually associated with water body covers, we use the threshold "NDVI $\leq$ 0" to exclude potential water bodies before implementing NAL. In this way, the range of NDVIs can be constrained as $NDVI \in (0, 1]$.

3.5. Extraction of human settlements with adaptive thresholds

The redistributed MPL data has greatly increased its intra-urban variability within sub-pixel resolutions, and is a useful indicator to characterize human activities and estimate human settlement areas. Extensive studies have used thresholding techniques to map urban and human settlement extent from NTL images at both regional and global scales due to their simplicity and intuitivity, especially when an optimal threshold is available (Imhoff et al., 1997). With the thresholding method, pixels with digital number (DN) values (e.g., NAL in this study) larger than a predefined value would be identified as "human settlement". However, there are several limitations using the thresholding methods employed in previous studies. First, it is difficult to define the optimal thresholds, and no single predefined threshold is valid to extract human settlement extent for various cities (Imhoff et al., 1997; Small, 2001; Xie and Weng, 2016). Second, empirical thresholds are incompatible across different spatiotemporal scales. In this paper, we proposed a robust training scheme using massive POIs data to adaptively define optimal thresholds for extracting human settlements. Specifically, we collected 21,789 training POI samples for Beijing, 19,227 training POI samples for Shanghai, and 11,817 training POI samples for Guangzhou. For each selected city, each POI sample P_i will have a corresponding NAL value N_i. After excluding the potential noises with $N_i = 0$, we then sorted the valid NAL data N_j from small to large order. The adaptive NAL threshold NT for each city was determined through Equations (4) and (5)

$$t = \lfloor \rho \cdot \mathrm{num}(N_j) \rfloor \tag{4}$$

$$NT = N_t \tag{5}$$

where $\mathrm{num}(N_j)$ denotes the total number of pixels in the NAL data, ρ denotes the cutting-off probability, which is assigned as 5% based on the experimental tests (see Results). t is the adaptive number order for the resorted NAL sequence.

3.6. National-scale human settlement extraction

The method above can be easily adjusted for redistributing the MPL data by other remotely sensed data. We further created the national-scale human settlement map with a 250-m spatial resolution by combining MPL data with time-series MODIS data. The max NDVI values were extracted from the one-year MODIS NDVI time series after noises being removed as elaborated in Section 3.1. The water layer (IGBP classification code: 0) from the MODIS collection 5 IGBP classification product (MCD12Q1) product (Friedl et al., 2010) was extracted and resampled to the same spatial resolution (250 m) as the MODIS NDVI data. Then, the extracted water layer was used to exclude water bodies from the MODIS NDVI data. Consequently, we could eliminate potential biases caused by low NDVI values of water bodies. Similar to the method described in Section 3.2, we further redistributed the MPL data using MODIS NDVI adjusted weights.

Given the differences of physical environment and socio-economic development in various areas of China, the usage of a uniform national-scale NAL threshold delineating human settlements will certainly result in the underestimation of small settlement areas and overestimation of those large ones. To solve this problem, we determined adaptive thresholds for each prefectural-level city in China by means of sample training with referenced POIs dataset. Similar to the method described in Section 3.4, for each prefectural-level city, each POI sample P_i will have a corresponding NAL value N_i. After excluding the potential noises with $N_i = 0$, we then sorted the valid NAL data N_j from small to large order. We assigned the cutting-off probability as 5%, and the adaptive NAL threshold NT for each prefectural-level city was determined through Equations (4) and (5).

3.7. Accuracy assessment of settlements extraction

To assess the performance of extracting human settlements quantitatively, we used POIs data as the ground truth reference to validate the accuracy. In this study, a total of 5.4 million POIs that are highly relevant to human daily life were acquired. In terms of accuracy assessment for 30-m human settlement mapping, we first created a grid mesh with a 30-m spatial resolution being consistent to that of the extracted human settlements and overlapped it with the POIs data. In this way, the total number of POIs within each grid can be calculated. Grids having a higher number of POIs are assumed to be with higher probabilities of human settlements. A cutting-off probability of upper 15% was assigned to define human settlements. For each city, the amount of POIs above the top 85 percentile was defined as the threshold, and grids with POIs larger than the threshold were defined as human settlements. Similarly, as for

Table 1
Brief description of datasets used for comparison.

Dataset	Spatial resolution	Year	Reference
Global human settlement layer (GHSL)	250 m	2015	(Pesaresi et al. 2013, 2016)
Global human built-up settlement extent (HBASE)	250 m	2010	Wang et al. (2017)
Global man-made impervious surface (GMIS)	250 m	2010	Brown de Colstoun et al. (2017)
LandScan	1000 m	2016	Dobson et al. (2000)

the accuracy assessment for 250-m human settlements in China, the initial grid mesh was generated with a 250-m spatial resolution, and the subsequent procedures were the same as that of accuracy assessment for 30-m human settlement mapping. In contrast, non-settlement samples were randomly generated outside those settlement samples. Specifically, there were 9,112 samples selected for Beijing, 4,030 samples for Shanghai, 8,879 samples for Guangzhou, and 34,600 samples for China. The overall accuracy accompanied with producer's accuracy and user's accuracy would be regarded as the major indicators of extraction accuracy.

3.8. Comparison with other datasets

We collected global human settlement layer (GHSL), global human built-up and settlement extent (HBASE), and global man-made impervious surface (GMIS) as comparable datasets (Table 1) to assess their accuracies. Additionally, we also collected the population dataset-LandScan (Table 1) to calculate the total population within the extracted human settlement layer, and then derived the percentage against the entire country. This indicator was further compared with the urbanization rate reported from National Bureau of Statistics of China in 2016.

4. Results

4.1. Deriving the redistributed NAL data

For each selected city, we fused the cloud-free fine-resolution Landsat OLI data and the coarse-resolution NDVI data derived from MOD13Q1 products to generate synthetic NDVI time series and calculate the max NDVI values from the fused intra-annual time series. The annual max NDVI data was chosen as the adjusted weights to downscale the original coarse-resolution MPL data according to the equations (2) and (3). As shown in the top row of Fig. 5, the MPL data could characterize the spatial distribution of active population very well in all three cities we examined. In addition, the MPL data recorded the total number of locating-request services from active users, thus averting the saturation of data values for each grid (1.2 km × 1.2 km). However, the ability of MPL data to characterize intra-urban variation was limited due to its coarse spatial resolution, especially for heterogeneous urban core areas (Fig. 5). In contrast, the NAL data could keep a consistent spatial distribution of active population with MPL data and capture the fine spatial details of NAL variations within urban areas (Fig. 5). With an intercomparison between the zoomed-in MPL and NAL data in the bottom rows of Fig. 5, we could clearly find that the MPL data, serving as a coarse-resolution spatial distribution of population density, was incapable to detect sub-pixel variations of population distribution, whereas the NAL data was able to characterize the fine-resolution distribution of population density and spatial allocation of human settlements.

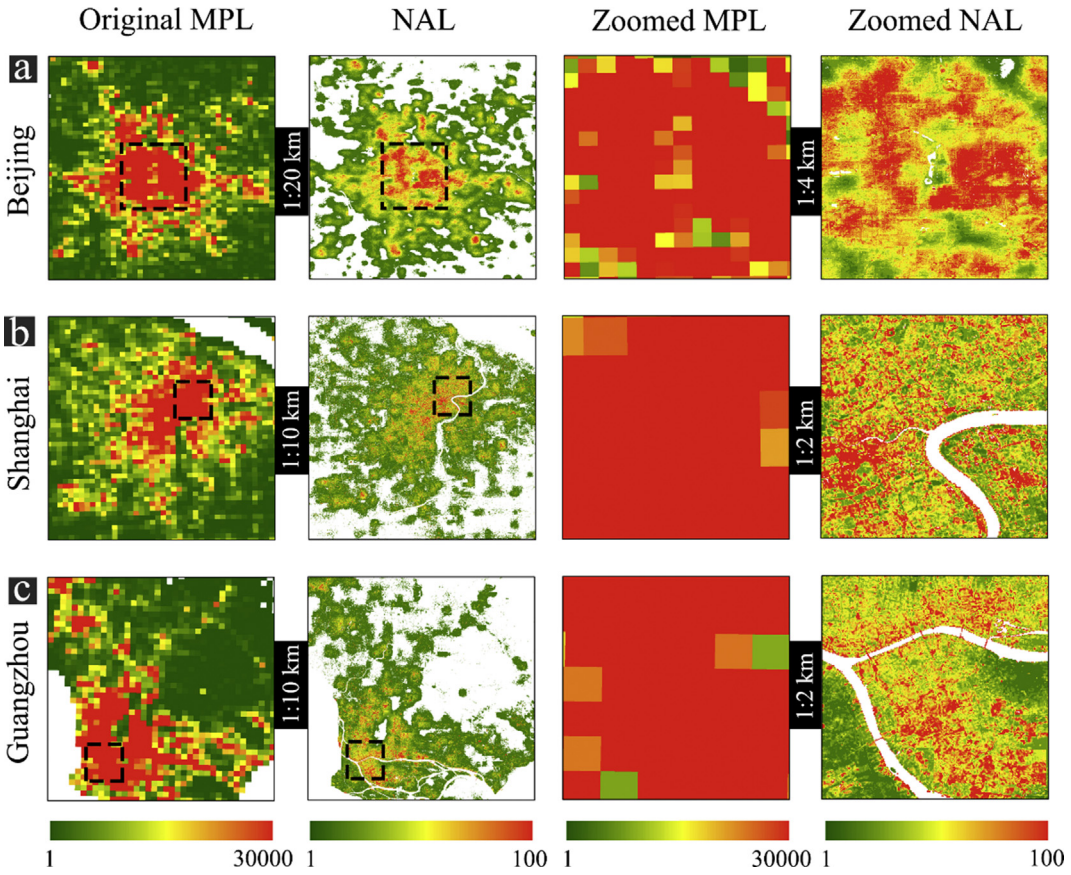

Fig. 5. Visualization of original mobile phone locating-request (MPL) data and NDVI-adjusted locating-request (NAL) data in the three selected cities (a) Beijing, (b) Shanghai, and (c) Guangzhou.

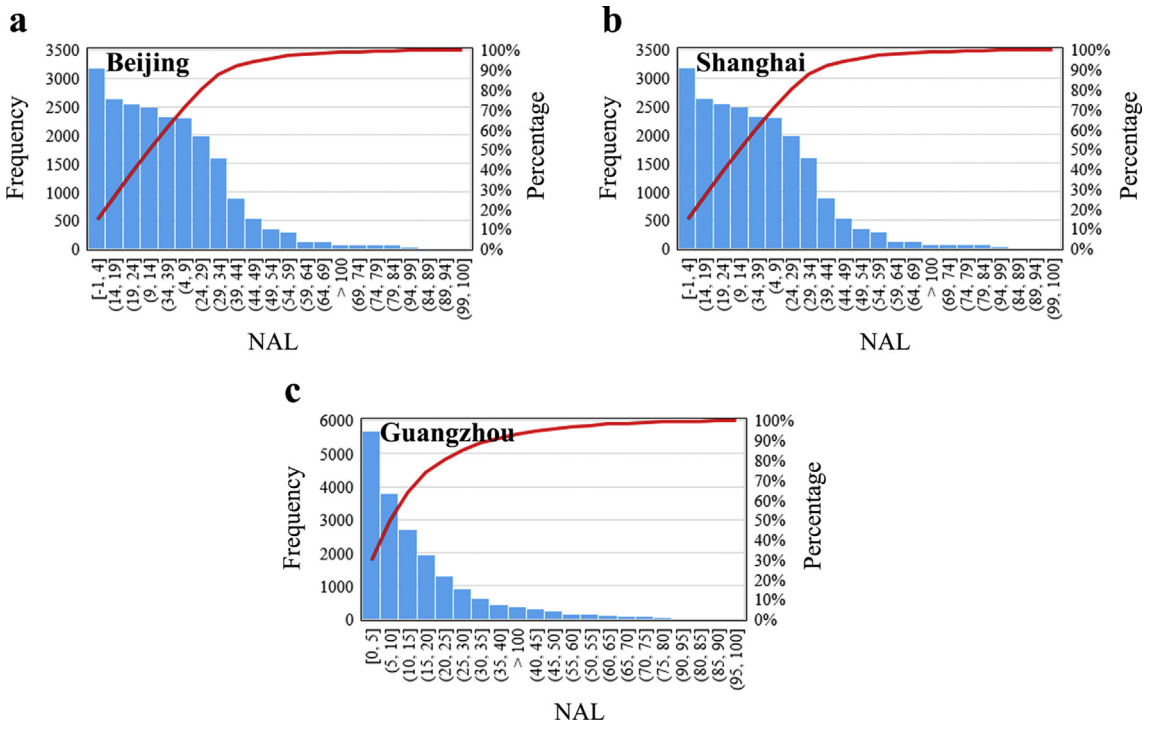

Fig. 6. The frequency and percentage of NAL values extracted by POIs training datasets in Beijing (a), Shanghai (b), and Guangzhou (c).

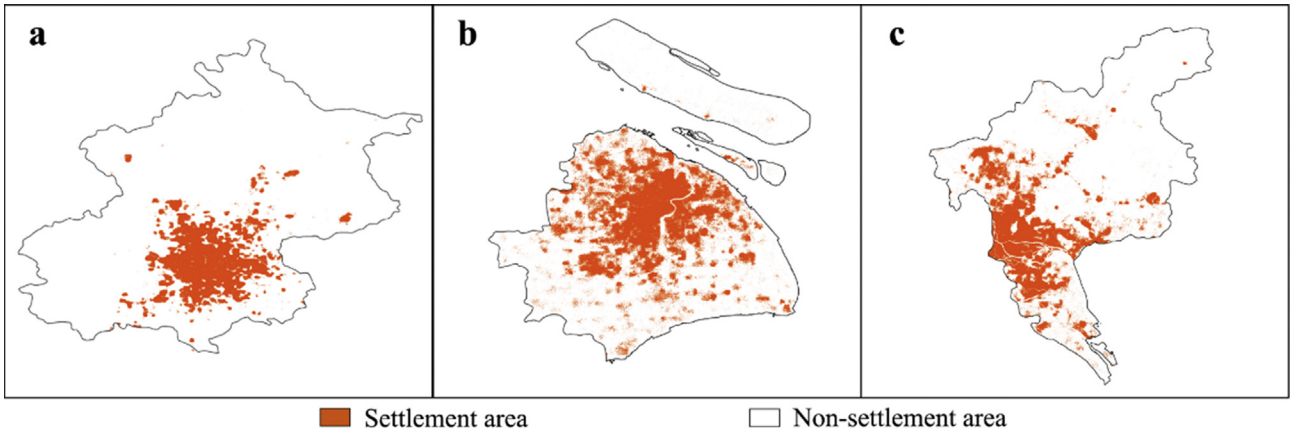

Fig. 7. Extracted human settlement areas for Beijing (a), Shanghai (b), and Guangzhou (c) in China.

4.2. Extracting human settlements using the NAL data

As the coarse-resolution MPL data was derived from averaging all daily records from March 14, 2016 to June 29, 2016, it represented the general geographic distribution of population by incorporating all the daily-, weekly-, and monthly-fluctuations of population movement. The NAL layer, obtained by redistributing coarse-resolution MPL using NDVI adjusted weights has already been approximate to the actual geographic extent of human settlement areas. As shown in Fig. 6, we found that the vast majority of the POIs training dataset extracted NAL values ranged from 1 to 100 for all the three selected cities. In order to exclude potential biases (e.g., negative values or null values) from the NAL, we assigned the cutting-off probability as 5% to refine NAL values extracted by the POIs training dataset.

After identifying the settlement area with the adaptive threshold *NT* for each selected city, we derived urban human settlement areas (Fig. 7). As shown in Fig. 7, the extracted results could generally reflect the detailed geographic distribution of human settlements in these three cities.

4.3. Validation of extraction accuracy using the POIs dataset

The quantitative accuracy of human settlement extraction was validated with randomly selected POI samples. As summarized in Table 2, experimental results showed that our method to extract human settlements achieved robust overall accuracies of 91.2% in Beijing, 90.0% in Shanghai, and 92.3% in Guangzhou. The Kappa coefficients were also above 0.82 for all three selected cities.

4.4. National-scale human settlement map in China

As shown in Fig. 8a, by extending the weighted redistributing method to the MPL and MODIS data, we could obtain the MODIS NDVI adjusted locating-request (NAL) data in China. The adaptive NAL threshold for each prefectural-level city was determined by means of sample training with referenced POIs dataset in Fig. 8b. We then extracted human settlement areas for each city and conducted the image mosaic to produce the national-scale human settlement map in China (Fig. 8c). Statistically,

Table 2
Confusion matrix and accuracy assessment of 30-m human settlement mapping in Beijing, Shanghai, and Guangzhou.

(1) Beijing	Overall accuracy: 91.2%; Kappa coefficient:0.82				
Class\Reference	Settlement	Non-settlement	Total	Pro. Acc. (%)	User Acc. (%)
Settlement	3,915	159	4,074	85.9	96.1
Non-settlement	641	4,397	5,038	96.5	87.3
Total	4,556	4,556	9,112		
(2) Shanghai	Overall accuracy: 90.0%; Kappa coefficient: 0.80				
Class\Reference	Settlement	Non-settlement	Total	Pro. Acc. (%)	User Acc. (%)
Settlement	1,678	67	1,745	83.3	96.2
Non-settlement	337	1,948	2,285	96.7	85.2
Total	2,015	2,015	4,030		
(3) Guangzhou	Overall accuracy: 92.3%; Kappa coefficient: 0.85				
Class\Reference	Settlement	Non-settlement	Total	Pro. Acc. (%)	User Acc. (%)
Settlement	3,827	77	3,904	86.2	98.0
Non-settlement	611	4,364	4,975	98.3	87.7
Total	4,438	4,441	8,879		

as for the 250-m human settlement mapping in China (Table 3), the overall accuracy was up to 95.2% with a Kappa coefficient of 0.90.

In the meantime, using the same 34,600 validation samples, the overall accuracies were 90.2% for GHSL, 89.2% for HBASE, and 89.7% for GMIS, which were all slightly lower than our extracted one. Compared with the entire country, Landscan-based population estimate is 64.7% within the extracted urban human settlements, which was quite close to the urbanization rate (i.e., 57.4% in 2016) in China (National Bureau of Statistics of China, 2017).

Table 3
Confusion matrix and accuracy assessment of 250-m human settlement mapping in China.

Class\Reference	Overall accuracy: 95.2%; Kappa coefficient: 0.90				
	Settlement	Non-settlement	Total	Pro. Acc. (%)	User Acc. (%)
Settlement	15,916	272	16,188	92.0%	98.3%
Non-settlement	1,384	17,028	18,412	98.4%	92.5%
Total	17,300	17,300	34,600		

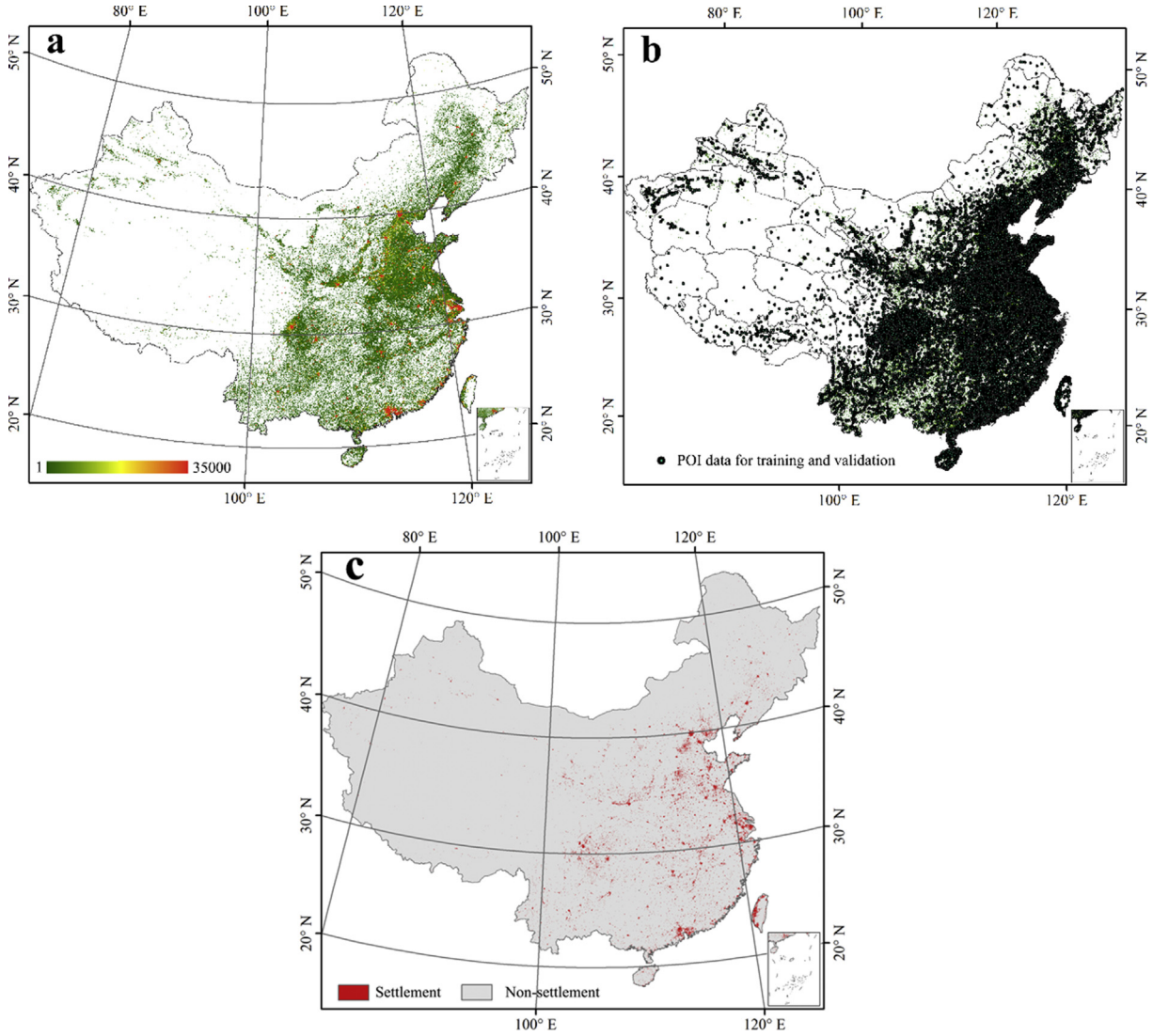

Fig. 8. MODIS NDVI adjusted locating-request (NAL) data in China (a), POI data for training and validation (b), and final national-scale human settlement extent with a 250-m spatial resolution (c).

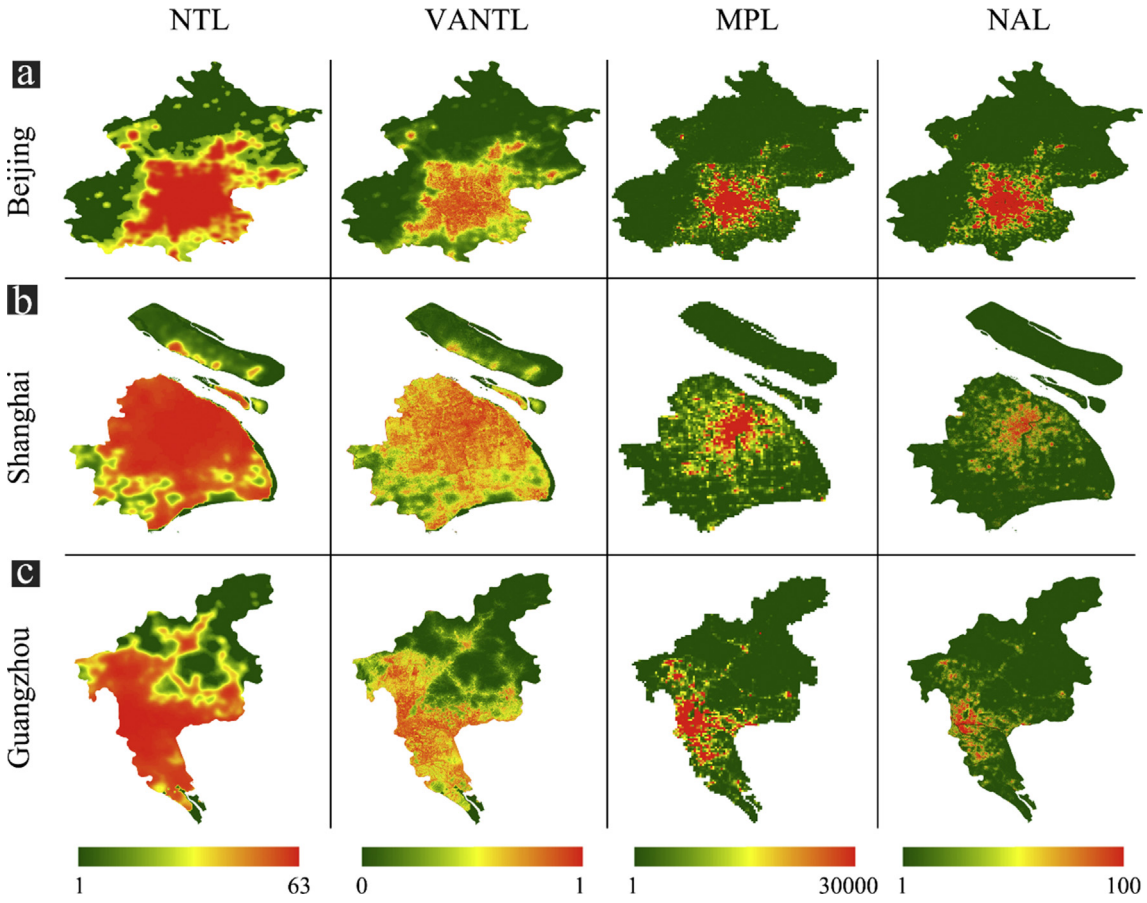

Fig. 9. Comparison of human settlements characterized by nighttime light data (NTL) and vegetation-adjusted nighttime light data (VANTL) derived from DMSP/OLS and VIIRS, mobile-phone locating-time data (MPL), and NDVI-adjusted mobile-phone locating-time data (NAL) in Beijing (a), Shanghai (b), and Guangzhou (c).

5. Discussion

5.1. Comparison between NTL and NAL based methods

Nighttime light (NTL) data have been extensively used to extract human settlement areas and related urban extent in previous approaches (Cao et al., 2009; Liu et al., 2012; Xie and Weng, 2016; Zhang et al., 2013). Here we further compared original NTL and vegetation adjusted NTL (VANTL) derived from DMSP-OLS and Suomi NPP VIIRS, original mobile phone locating-time data (MPL), and NDVI-adjusted locating-time data (NAL) simultaneously in three selected cities. As shown in Fig. 9, all six indicators captured the general spatial patterns of human settlement distribution in different cities. However, the blooming effect of NTL data was serious, thus leading to an inevitable overestimation of human settlement extraction. Integrated with fine-resolution NDVI data, VANTL was improved to be useful in characterizing human settlements with more spatial details, but it was still limited by the blooming effects of NTL data and would overestimate the extent of human settlements. Due to the coarse spatial resolution and easy-to-reach oversaturation, the blooming effect was especially serious for the characterization of human settlements using only DMSP-OLS data (the first column in Fig. 9). With the improvement of spatial resolution and the enlarged range of nighttime light signals, the blooming effect was eliminated significantly for VIIRS data (the third column in Fig. 9), but it still led to biases in overestimating the extent of human settlements outside the urban cores. In contrast, MPL could perfectly solve the long-existing problems of NTL data including the saturation of data value, and blooming effects, which provided a possible alternative to characterize the extent and intra-structure of our human settlements.

5.2. Implications and uncertainties of methods

Geospatial big data have been widely recognized in providing opportunities for the characterization of human activities. In this study, with the unique geotagged information from the Tencent MPL data, we dig out the geographic distribution of people with unprecedented spatial details. By incorporating the population distribution inferred from the MPL data with remotely sensed data, we have a new way to extract human settlements by considering both physical and anthropogenic attributes. In addition to the abovementioned merits, some potential concerns about our research methods and results need to be addressed. First, although the negative correlation between NDVI and MPL has been verified to be significant in all three cities, its variation accountability remains to be at a low level because of the biased noises from massive samples. Better refining the adjusted weights that redistribute coarse-resolution MPL data into fine-resolution grids requires to integrate with more input variables, such as building density and land surface temperature. Second, the extracted human settlements using our method can well exclude the broad roads in rural areas, but our current human settlement map cannot exclude roads or streets within the urban cores since the MPL data are massively recorded at these areas with dense human activities. In contrast, human settlements in rural areas with less active MPL records will be underestimated. Therefore, in a broader view, our nationwide human settlement mapping is more focused on urban areas. Third, the Tencent-based MPL data tend to leave out some population groups of the society because the children, the elderly, and the poor are less-frequent active users. Nevertheless, the current data can still well quantify population distribution patterns on account to the massive volume of data records. The MPL data has been recorded and released

since late 2015, therefore, we cannot produce historical human settlement maps before 2015 using current data sources. However, we can incorporate other possible geotagged information from mobile-phone towers and other location-based social media data such as Weibo, Twitters, and Flickr that have longer-term historical records. The production of time-series human settlement maps from the past to date is still an open question for our future research.

6. Conclusions

With the integration of location-based and remotely sensed data, our study provides a novel approach to extract human settlements by combining the physical and socio-economic properties simultaneously. Experimental tests in selected sites with a medium resolution (30 m) and in a national scale with a coarse resolution (250 m) were verified to map human settlement extent accurately. In addition, the proposed method can be easily adjusted with multi-scale remotely sensed data and applied to human settlement extraction at different spatial scales.

Declaration of competing interest

The authors declare that they have no known competing financial interests or personal relationships that could have appeared to influence the work reported in this paper.

Acknowledgements

The authors thank Tencent Inc. for making the mobile phone location data publicly available, and thank two anonymous reviewers and editors for providing valuable suggestions and comments, which are greatly helpful in improving this manuscript. This work was supported by the Ministry of Science and Technology of China under the National Key Research and Development Program (2016YFA0600104) and by donations from Delos Living LLC and the Cyrus Tang Foundation to Tsinghua University.

Appendix A. Supplementary data

Supplementary data to this article can be found online at https://doi.org/10.1016/j.srs.2020.100003.

References

Brown de Colstoun, E., Huang, C., Wang, P., Tilton, J., Tan, B., Phillips, J., Niemczura, S., Ling, P., Wolfe, R., 2017. Global Man-Made Impervious Surface (GMIS) Dataset from Landsat. NASA Socioeconomic Data and Applications Center (SEDAC), *Palisades, NY, USA*.

Cai, J., Huang, B., Song, Y., 2017. Using multi-source geospatial big data to identify the structure of polycentric cities. Remote Sens. Environ. 202, 210–221.

Cao, X., Chen, J., Imura, H., Higashi, O., 2009. A SVM-based method to extract urban areas from DMSP-OLS and SPOT VGT data. Remote Sens. Environ. 113, 2205–2209.

Carter, J.G., Cavan, G., Connelly, A., Guy, S., Handley, J., Kazmierczak, A., 2015. Climate change and the city: building capacity for urban adaptation. Prog. Plann. 95, 1–66.

Chen, B., Chen, L., Huang, B., Michishita, R., Xu, B., 2018a. Dynamic monitoring of the Poyang Lake wetland by integrating Landsat and MODIS observations. ISPRS J. Photogrammetry Remote Sens. 139, 75–87.

Chen, B., Huang, B., Xu, B., 2017. Multi-source remotely sensed data fusion for improving land cover classification. ISPRS J. Photogrammetry Remote Sens. 124, 27–39.

Chen, B., Song, Y., Jiang, T., Chen, Z., Huang, B., Xu, B., 2018b. Real-time estimation of population exposure to PM2. 5 using Mobile-and station-based big data. Int. J. Environ. Res. Publ. Health 15, 573.

Chen, B., Song, Y., Kwan, M.-P., Huang, B., Xu, B., 2018c. How do people in different places experience different levels of air pollution? Using worldwide Chinese as a lens. Environ. Pollut. 238, 874–883.

Deville, P., Linard, C., Martin, S., Gilbert, M., Stevens, F.R., Gaughan, A.E., Blondel, V.D., Tatem, A.J., 2014. Dynamic population mapping using mobile phone data. Proc. Natl. Acad. Sci. Unit. States Am. 111, 15888–15893.

Dobson, J.E., Bright, E.A., Coleman, P.R., Durfee, R.C., Worley, B.A., 2000. LandScan: a global population database for estimating populations at risk. Photogramm. Eng. Rem. Sens. 66, 849–857.

Elvidge, C.D., Imhoff, M.L., Baugh, K.E., Hobson, V.R., Nelson, I., Safran, J., Dietz, J.B., Tuttle, B.T., 2001. Night-time lights of the world: 1994–1995. ISPRS J. Photogrammetry Remote Sens. 56, 81–99.

Esch, T., Marconcini, M., Felbier, A., Roth, A., Heldens, W., Huber, M., Schwinger, M., Taubenböck, H., Müller, A., Dech, S., 2013. Urban footprint processor—fully automated processing chain generating settlement masks from global data of the TanDEM-X mission. Geosci. Rem. Sens. Lett. IEEE 10, 1617–1621.

Esch, T., Thiel, M., Schenk, A., Roth, A., Muller, A., Dech, S., 2010. Delineation of urban footprints from TerraSAR-X data by analyzing speckle characteristics and intensity information. IEEE Trans. Geosci. Rem. Sens. 48, 905–916.

Frias-Martinez, V., Soto, V., Hohwald, H., Frias-Martinez, E., 2012. Characterizing urban landscapes using geolocated tweets. In: Privacy, Security, Risk and Trust (PASSAT), 2012 International Conference on and 2012 International Confernece on Social Computing (SocialCom). IEEE, pp. 239–248.

Friedl, M.A., Sulla-Menashe, D., Tan, B., Schneider, A., Ramankutty, N., Sibley, A., Huang, X., 2010. MODIS Collection 5 global land cover: algorithm refinements and characterization of new datasets. Remote Sens. Environ. 114, 168–182.

Gamba, P., Aldrighi, M., Stasolla, M., 2011. Robust extraction of urban area extents in HR and VHR SAR images. IEEE J. Select. Topics Appl. Earth Observ. Remote Sens. 4, 27–34.

Goldblatt, R., Stuhlmacher, M.F., Tellman, B., Clinton, N., Hanson, G., Georgescu, M., Wang, C., Serrano-Candela, F., Khandelwal, A.K., Cheng, W.-H., 2018. Using Landsat and nighttime lights for supervised pixel-based image classification of urban land cover. Remote Sens. Environ. 205, 253–275.

Huang, Q., He, C., Gao, B., Yang, Y., Liu, Z., Zhao, Y., Dou, Y., 2015. Detecting the 20 year city-size dynamics in China with a rank clock approach and DMSP/OLS nighttime data. Landsc. Urban Plann. 137, 138–148.

Imhoff, M.L., Lawrence, W.T., Stutzer, D.C., Elvidge, C.D., 1997. A technique for using composite DMSP/OLS "city lights" satellite data to map urban area. Remote Sens. Environ. 61, 361–370.

Jin, Z., Xu, B., 2013. A novel compound smoother: RMMEH to reconstruct MODIS NDVI time series. Geosci. Rem. Sens. Lett. IEEE 10, 942–946.

Jurdak, R., Zhao, K., Liu, J., AbouJaoude, M., Cameron, M., Newth, D., 2015. Understanding human mobility from Twitter. PloS One 10, e0131469.

Kaplan, A.M., Haenlein, M., 2010. Users of the world, unite! the challenges and opportunities of Social Media. Bus. Horiz. 53, 59–68.

Kawamura, M., 1996. Relation between social and environmental conditions in Colombo Sri Lanka and the urban index estimated by satellite remote sensing data. In: Proc. 51st Annual Conference of the Japan Society of Civil Engineers, pp. 190–191.

Klepeis, N.E., Nelson, W.C., Ott, W.R., Robinson, J.P., Tsang, A.M., Switzer, P., Behar, J.V., Hern, S.C., Engelmann, W.H., 2001. The National Human Activity Pattern Survey (NHAPS): a resource for assessing exposure to environmental pollutants. J. Expo. Anal. Environ. Epidemiol. 11, 231–252.

Li, X., Gong, P., 2016. An "exclusion-inclusion" framework for extracting human settlements in rapidly developing regions of China from Landsat images. Remote Sens. Environ. 186, 286–296.

Liu, Z., He, C., Zhang, Q., Huang, Q., Yang, Y., 2012. Extracting the dynamics of urban expansion in China using DMSP-OLS nighttime light data from 1992 to 2008. Landsc. Urban Plann. 106, 62–72.

Lu, D., Li, G., Moran, E., Batistella, M., Freitas, C.C., 2011. Mapping impervious surfaces with the integrated use of Landsat Thematic Mapper and radar data: a case study in an urban–rural landscape in the Brazilian Amazon. ISPRS J. Photogrammetry Remote Sens. 66, 798–808.

Lu, D., Tian, H., Zhou, G., Ge, H., 2008. Regional mapping of human settlements in southeastern China with multisensor remotely sensed data. Remote Sens. Environ. 112, 3668–3679.

Lu, D., Weng, Q., 2006. Use of impervious surface in urban land-use classification. Remote Sens. Environ. 102, 146–160.

Lu, D., Weng, Q., 2009. Extraction of urban impervious surfaces from an IKONOS image. Int. J. Rem. Sens. 30, 1297–1311.

Masek, J.G., Vermote, E.F., Saleous, N., Wolfe, R., Hall, F.G., Huemmrich, F., Gao, F., Kutler, J., Lim, T.K, 2013. LEDAPS Calibration, Reflectance, Atmospheric Correction Preprocessing Code, Version 2. Model product. ORNL DAAC. Oak Ridge, Tennessee, USA. https://doi.org/10.3334/ORNLDAAC/1146.

Matsuoka, R.H., Kaplan, R., 2008. People needs in the urban landscape: analysis of landscape and urban planning contributions. Landsc. Urban Plann. 84, 7–19.

National Bureau of Statistics of China, 2017. Urbanization in China. http://www.stats.gov.cn/.

Patel, N.N., Angiuli, E., Gamba, P., Gaughan, A., Lisini, G., Stevens, F.R., Tatem, A.J., Trianni, G., 2015. Multitemporal settlement and population mapping from landsat using Google Earth engine. Int. J. Appl. Earth Obs. Geoinf. 35, 199–208. Part B.

Pauleit, S., Ennos, R., Golding, Y., 2005. Modeling the environmental impacts of urban land use and land cover change—a study in Merseyside, UK. Landsc. Urban Plann. 71, 295–310.

Pelizari, P.A., Spröhnle, K., Geiß, C., Schoepfer, E., Plank, S., Taubenböck, H., 2018. Multi-sensor feature fusion for very high spatial resolution built-up area extraction in temporary settlements. Remote Sens. Environ. 209, 793–807.

Pesaresi, M., Ehrlich, D., Florczyk, A.J., Freire, S., Julea, A., Kemper, T., Syrris, V., 2016. The global human settlement layer from landsat imagery. In: 2016 IEEE International Geoscience and Remote Sensing Symposium (IGARSS), pp. 7276–7279.

Pesaresi, M., Huadong, G., Blaes, X., Ehrlich, D., Ferri, S., Gueguen, L., Halkia, M., Kauffmann, M., Kemper, T., Lu, L., 2013. A global human settlement layer from optical HR/VHR RS data: concept and first results. IEEE J. Select. Topics Appl. Earth Observ. Remote Sens. 6, 2102–2131.

Ridd, M.K., Hipple, J.M., 2006. Remote Sensing of Human Settlements. American Society of Photogrammetry and Remote Sensing, Bethesda, Maryland.

Rouse, J., Haas, R., Schell, J., Deering, D., 1974. Monitoring Vegetation Systems in the Great Plains with ERTS, vol. 351. NASA Special Publication, p. 309.

Salentinig, A., Gamba, P., 2015. Combining SAR-based and multispectral-based extractions to map urban areas at multiple spatial resolutions. IEEE Geosci. Remote Sens. Mag. 3, 100–112.
Schneider, A., Friedl, M.A., Potere, D., 2010. Mapping global urban areas using MODIS 500-m data: new methods and datasets based on 'urban ecoregions'. Remote Sens. Environ. 114, 1733–1746.
Shao, M., Tang, X., Zhang, Y., Li, W., 2006. City clusters in China: air and surface water pollution. Front. Ecol. Environ. 4, 353–361.
Small, C., 2001. Estimation of urban vegetation abundance by spectral mixture analysis. Int. J. Rem. Sens. 22, 1305–1334.
Song, Y., Huang, B., Cai, J., Chen, B., 2018. Dynamic assessments of population exposure to urban greenspace using multi-source big data. Sci. Total Environ. 634, 1315–1325.
Song, Y., Huang, B., He, Q., Chen, B., Wei, J., Mahmood, R., 2019. Dynamic assessment of PM2. 5 exposure and health risk using remote sensing and geo-spatial big data. Environ. Pollut. 253, 288–296.
Steiger, E., Westerholt, R., Resch, B., Zipf, A., 2015. Twitter as an indicator for whereabouts of people? Correlating Twitter with UK census data. Comput. Environ. Urban Syst. 54, 255–265.
Tencent, 2016. Annual report. https://data.qq.com/reports.
Tian, H., Huang, S., Zhou, S., Bi, P., Yang, Z., Li, X., Chen, L., Cazelles, B., Yang, J., Luo, L., Jing, Q., Yuan, W., Pei, Y., Sun, Z., Yue, T., Kwan, M.-P., Liu, Q., Wang, M., Tong, S., Brownstein, J.S., Xu, B., 2016. Surface water areas significantly impacted 2014 dengue outbreaks in Guangzhou, China. Environ. Res. 150, 299–305.
Wang, P., Huang, C., Brown de Colstoun, E., Tilton, J., Tan, B., 2017. Global Human Built-Up and Settlement Extent (HBASE) Dataset from Landsat. NASA Socioeconomic Data and Applications Center (SEDAC), *Palisades, NY, USA*.
Waseem, S., Khayyam, U., 2019. Loss of vegetative cover and increased land surface temperature: a case study of Islamabad, Pakistan. J. Clean. Prod. 234, 972–983.
Weng, Q., 2012. Remote sensing of impervious surfaces in the urban areas: requirements, methods, and trends. Remote Sens. Environ. 117, 34–49.
Weng, Q., Lu, D., Liang, B., 2006. Urban surface biophysical descriptors and land surface temperature variations. Photogramm. Eng. Rem. Sens. 72, 1275–1286.
Weng, Q., Lu, D., Schubring, J., 2004. Estimation of land surface temperature–vegetation abundance relationship for urban heat island studies. Remote Sens. Environ. 89, 467–483.
Xie, Y., Weng, Q., 2016. Updating urban extents with nighttime light imagery by using an object-based thresholding method. Remote Sens. Environ. 187, 1–13.
Xu, B., Yang, J., Zhang, Y., Gong, P., 2016. Healthy cities in China: a lancet commission. Lancet 388, 1863–1864.
Xu, H., 2008. A new index for delineating built-up land features in satellite imagery. Int. J. Rem. Sens. 29, 4269–4276.
Zha, Y., Gao, J., Ni, S., 2003. Use of normalized difference built-up index in automatically mapping urban areas from TM imagery. Int. J. Rem. Sens. 24, 583–594.
Zhang, Q., Schaaf, C., Seto, K.C., 2013. The Vegetation Adjusted NTL Urban Index: a new approach to reduce saturation and increase variation in nighttime luminosity. Remote Sens. Environ. 129, 32–41.
Zhang, X., Li, P., 2018. A temperature and vegetation adjusted NTL urban index for urban area mapping and analysis. ISPRS J. Photogrammetry Remote Sens. 135, 93–111.
Zhang, X., Li, P., Cai, C., 2015. Regional urban extent extraction using multi-sensor data and one-class classification. Rem. Sens. 7, 7671–7694.
Zhang, Y., Wang, T., Cai, C., Li, C., Liu, Y., Bao, Y., Guan, W., 2016. Landscape pattern and transition under natural and anthropogenic disturbance in an arid region of northwestern China. Int. J. Appl. Earth Obs. Geoinf. 44, 1–10.
Zhou, L., Dickinson, R.E., Tian, Y., Fang, J., Li, Q., Kaufmann, R.K., Tucker, C.J., Myneni, R.B., 2004. Evidence for a significant urbanization effect on climate in China. Proc. Natl. Acad. Sci. Unit. States Am. 101, 9540–9544.
Zhou, X., Chen, H., 2018. Impact of urbanization-related land use land cover changes and urban morphology changes on the urban heat island phenomenon. Sci. Total Environ. 635, 1467–1476.